Journal of Applied Polymer Science

Simplified modeling of the electrospinning process from the stable jet region to the unstable region for predicting the final nanofiber diameter

Nagham Ismail,[1] Fouad Junior Maksoud,[2] Nesreen Ghaddar,[1] Kamel Ghali,[1] Ali Tehrani-Bagha[2]

[1]Mechanical Engineering Department, American University of Beirut, P.O. Box 11-0236, Beirut 1107-2020, Lebanon

[2]Department of Chemical and Petroleum Engineering, American University of Beirut, P.O. Box 11-236, Beirut 1107-2020, Lebanon

Correspondence to: N. Ghaddar (E-mail: farah@aub.edu.lb)

ABSTRACT: Electrospinning allows the production of ultrafine nanofibers through the stretching of a charged polymer jet with an external electrostatic field. In this study, we derived a simplified and accurate model relating the processing parameters, including the solution volumetric flow rate (Q), the applied electric field (E), and the polymer concentration, to the final fiber diameter. The model takes into consideration the jet behavior starting at the stable region and moving to the bending instability region. We validated the model experimentally by performing the electrospinning process with a polyacrylonitrile/*N*,*N*-dimethylformamide solution with different ranges of concentrations (8–11 wt %), Qs (900–1320 μL/h), and Es (88,889–113,889 V/m). The final fiber diameter was measured with scanning electron microscopy. The model predicted the fiber diameter with a relative error of less than 10%. Moreover, a 30% increase in Q resulted in a 15% increase in the fiber diameter, whereas a 30% increase in E resulted in a 14% decrease in the fiber diameter. © 2016 Wiley Periodicals, Inc. J. Appl. Polym. Sci. **2016**, *133*, 44112.

KEYWORDS: conducting polymers; electrospinning; fibers

Received 27 March 2016; accepted 22 June 2016
DOI: 10.1002/app.44112

INTRODUCTION

Electrospinning is a promising technique for producing nanofibers by subjecting a polymeric solution to an electric field (E).[1] In recent years, various polymers, including nylon, polyurethane, and polyacrylonitrile (PAN), have been successfully electrospun into ultrafine fibers.[2–4] Indeed, the increased popularity of electrospinning has arisen from the simplicity of the process and the ability to produce a relatively thin nonwoven mesh/membrane.[5] Electrospun nanofibrous mesh has a large surface area because the nanodiameters of their fibers allow their use in the filtration of subparticles and in the adsorption of biological and chemical warfare gases, in protective clothing, in the medical industry, and in jet printing.[6,7]

Because the purpose of electrospinning is to produce a nanofibrous mesh, it is of interest to predict via modeling the final fiber diameter of single-nozzle electrospun fibers. A model that predicts the final fiber diameter can be used to control the electrospinning process to achieve desired fiber morphology, porosity, and physical characteristics and to improve the electrospinning efficiency.[8] Recently, different models have been developed for the electrospinning process. The modeling approaches in the literature[9–17] divide the jet into stable and unstable regions, where different governing equations are used. The focus of literature modeling is more on the portion of the electrified jet beyond the stable region where the jet becomes no longer visible.[9]

The stable jet region has been modeled as an electrified jet subjected to stretching by an external E. The basic principles for modeling electrified jets were developed by Taylor,[10] who discovered that it is impossible to account for most electrical phenomena under the assumption that the fluid is either a perfect dielectric or a perfect conductor. The reason is that any perfect dielectric fluid still contains a nonzero free charge density that lives on the interface between the fluid and the surrounding gas. The Taylor model was improved by the inclusion of the effects of jet stretching, charge transport, and E; this is called the slender body model.[11] In the slender body model, regular perturbations for long jets can be expanded with the integral formulations, Taylor's series expansions, weighted residuals, and variational principles. Feng[12] derived a modified model to avoid the instability issues of the slender body model. In Feng's model, the jet is represented by four steady-state equations: the continuity equation, momentum conservation, charge conservation, and Coulomb's law. However, generalized Newtonian constitutive relations are used for the

viscous normal stress difference. Roozemond[13] expanded Feng's model to account for the viscoelastic properties of the polymer solution fluid. Recently, Helgeson *et al.*[14] derived a simplified approach for the first electrospinning stable stage and developed a correlation that predicts the electrospun fiber diameter. However, the models of Roozemond,[13] Feng,[12] and Helgeson *et al.*[14] are only applicable in the stable region of electrospinning, where the jet is still straight. The stable region is a relatively small distance compared to the total distance from the needle (nozzle) tip to the collector, but the stable region affects the prediction of the final fiber diameter. Moreover, limiting the electrospinning process to the stable region cannot produce a nanometer fiber diameter, and the fibers leaving the stable region normally have diameters on the order of micrometers. Thus, it is of interest to connect the stable region model to the second jet flow stage of electrospinning, in which bending instability region occurs, to predict the final fiber diameter.

The model of the second stage of electrospinning (in the unstable region) presents a major challenge in the physics of the electrically driven jet.[15] To model the bending instability region, Hohman *et al.*[16] performed a linear stability analysis of the slender charged fluid jet with the leaky dielectric properties in a tangential *E*. However, the linear stability analysis covers only the early stages of the evolution of the instability; this is not usually the case for single-nozzle electrospinning.[15] Another model of electrospinning was developed by Yarin *et al.*,[17,18] who modeled a segment of the jet by a viscoelastic dumbbell. In their model, significant assumption is taken, where bending is assumed to be driven by charge repulsion and resisted by the solution elasticity. However, their model does not include any asymptotic analysis to predict the magnitude of the terminal diameter that the whipping jet can reach, and this necessitates a high computational cost because of its complex numerical solution.[18,19]

Therefore, there is a need to derive a simple and accurate model that relates the processing parameters to the final fiber properties. Fridrikh *et al.*[20] derived a simple expression of the final fiber diameter in electrospinning on the basis of the forces dominating the final stages of bending instabilities in electrospinning. Their expression of the final fiber diameter includes a characteristic length parameter (χ) that is not calculated. Fridrikh *et al.*[20] reported an arbitrary wide range for χ and did not report any systematic method of its calculation. It is of interest that χ is influenced by the first stage of electrospinning, which is the stable jet. By neglecting the relation between χ and the stable jet parameters, the Fridrikh *et al.*[20] model was reported to have an average relative error of 20% for a PAN solution.

The objective of this study was to develop a combined simplified model that covers the two connected stages of electrospinning: stable and unstable jets. Such a predictive model will help in predicting the behavior of different polymer–solvent solutions and different processing parameters and in guiding experimental studies. The novelty of such an approach arises from the prediction of the final fiber diameter by the modeling of the straight jet and the relation of the stable properties of the stable jet to the unstable region model. The combined model incorporates all of the physics of the jet during the electrospinning process. Moreover, the complete model was validated experimentally for different parameters [volumetric flow rate (Q), E, and concentration] through a comparison of the measured values to the predicted fiber diameter. The model results were also compared with other published models and experiments.

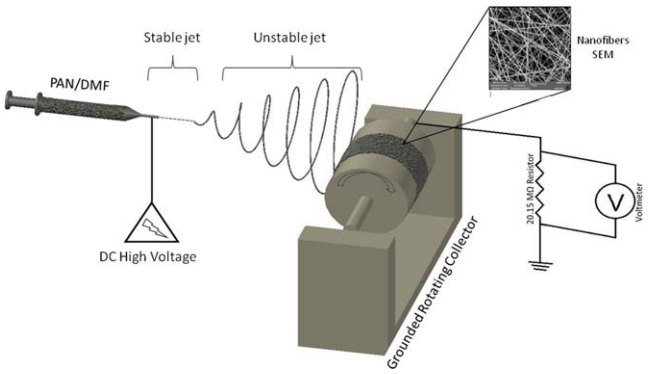

Figure 1. Schematic of the experimental setup for electrospinning. DC = direct current. [Color figure can be viewed in the online issue, which is available at wileyonlinelibrary.com.]

EXPERIMENTAL

The approach in this study combined the stable properties of the stable jet to the unstable region model in a simplified model that predicts the final fiber diameter as a function of the electrospinning processing parameters. The combined simplified model was based on the solution of electrohydrodynamics equations, including equations for mass, momentum, charge conservation, and Coulomb's law, inside the fluid jet in the initial stable jet region, and it uses the stable jet properties [r_{sj} and final stable jet surface charge density (ς_{sj})] in the unstable jet region. In the stable jet region, the electrohydrodynamics equations are solved for a certain length, which designates the straight jet of the stable region. Afterward, the equation of motion in the unstable region is simplified on the basis of some relevant assumptions and is solved with the stable region properties predicted.

To validate the simplified model, several experiments were performed for different electrospinning parameters (Q, E, and polymer concentration). For each experiment, the electric current (I) and the final fiber diameter were measured so they could be compared with the value predicted by the model for each input set.

Basic Equations of an Electrospun Polymer Jet

A scheme showing the horizontal electrospinning setup is shown in Figure 1. The electrically conducting polymer solution, characterized by its density (ρ), surface tension (γ), dynamic viscosity (η), electrical conductivity (k), and dielectric constant, was pumped at a Q out of an orifice of a metal syringe with an initial radius r_0. A high voltage (2–20 kV) was applied between the needle and the grounded collector, which were separated by a distance equal to L, where $L >> r_0$. Upon the application of a high voltage, the electrodes generated a homogeneous electric field strength (E_∞) directed horizontally from the needle toward the collector.[21] This E generated a tangential force on the charges distributed at the jet surface. The tangential force caused the jet to emanate

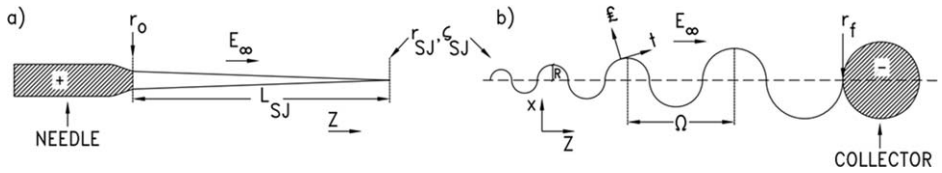

Figure 2. Physical model of the electrospinning process: (a) stable jet and (b) bending instability. t: tangential direction; ς: normal direction

from the tip of a needle as a charged liquid cone. Afterward, it was transformed into a thin straight jet for a relatively short distance [stable jet length (L_{sj})] and then became erratic and unstable because of bending instability.

The behavior of an electrospun polymer is generally described by electrohydrodynamics equations, which include equations for mass, momentum, charge conservation, and Coulomb's law inside the fluid jet. These equations relate the jet radius (r), jet velocity (v), surface charge density (ς), and E to the axial distance (z). The physical model of the electrospun jet is shown in Figure 2 and divides the jet into two regions: (1) the stable region and (2) the bending instability region. The physical parameters that influence the behavior of the electrospun jet in both regions include both the jet solution properties and the electrospinning process parameters. The solution properties are the effective η, k, γ, the electrical permittivity ($\bar{\varepsilon}$), and ρ. They are related to the chosen polymer–solvent solution and the weight concentration of the polymer in this solution. The electrospinning processing parameters are the jet Q, E_∞ [computed from the ratio of the difference in voltage (ΔV) to the distance L from the tip to the collector $\Delta V/L$], and r_0 of the nozzle. The processing parameters E_∞ and Q and the solution k can be used to determine I flowing through the jet with current–voltage relationships reported for electrospinning experiments.[16,21–25] Although I can be measured experimentally[23] by the connection of a resistor between the collector and the ground, Bhattacharjee *et al.*[25] reported that I measured in electrospinning scales as the product $E_\infty Q^{0.5} k^{0.4}$ for wide polymer solutions in an organic solvent could be expressed as follows:

$$I = aE_\infty Q^{0.5} k^{0.4} \tag{1}$$

where a is an empirical constant predicted as a function of the polymer solution and the geometrical characteristics of the electrospinning device. Equation (1) eliminates the need to perform measurements for the current once a is determined for a given polymer solution. In what follows, the governing equations of both jet regions are presented and are followed by the combined numerical/analytical solution methodology.

Stable Jet Region. In the stable jet region, shown in Figure 2(a), the liquid was characterized by weak conduction, and therefore, the leaky electric model applied.[12] The slender body approximations were adopted to model the stable viscoelastic electrospun jet where the flow was simplified to a nonuniform elongation with all quantities depending only on z. In addition, a negligible effect of solvent evaporation from the jet was assumed. Moreover, the viscoelastic Giesekus constitutive laws were used to determine the relation between the viscous stresses in the momentum equation. The Giesekus model adds quadratic nonlinearity and considers that the deviatoric stress is the sum of the solvent and polymer stresses.[26]

The current model for the stable jet region was based on Feng's model,[12] where the jet is governed by four steady-state equations representing the conservation of mass, electric charges, linear momentum balance, and Coulomb's law. With the stated assumptions, the equations governing the stable jet are applicable for a specific length, which is L_{sj}. However, L_{sj} is a function of the stable model output parameters.[27] To calculate L_{sj}, He *et al.*[27] provided a rational theory considering a steady-state flow of an infinite viscous jet pulled from a capillary orifice and accelerated by a constant external E. Because the electrical force is dominant over other forces in the stable jet, the bending instability occurs when the conductive and convective Is are equal. He *et al.*[27] derived the equation of L_{sj} on the basis of this criterion as follows:

$$L_{sj} = \frac{4kQ^3}{\pi\rho^2 I^2}\left[\left(\frac{2\varsigma_{sj}Q}{\pi K \rho E_{sj}}\right)^{-2/3} - r_0^{-2}\right] \tag{2}$$

Therefore, the electrohydrodynamic equations were derived for an arbitrarily assumed L_{sj}, which would be corrected iteratively on the basis of model output, as is described in the methodology of the Feng[12] model.

The mass conservation equation for the jet is as follows:

$$\pi r^2 v = Q \tag{3}$$

where r and v are measured at z. The charge conservation balance is given by[12]

$$2\pi r\varsigma v + \pi r^2 kE = I \tag{4}$$

The forces applied on the small control volume shown in Figure 3 are the tangential and the normal components of the electric force, the viscous stress, and γ. The linear momentum equation in the axial direction is given by[12]

$$\left(\tau_t^e - \tau_n^e \frac{dr}{dz}\right)2\pi r + \frac{d}{dz}[\pi r^2(\tau_{zz} - p)] + \frac{\gamma}{r}\frac{dr}{dz}2\pi r + \rho g \pi r^2 = \frac{d(\rho\pi r^2 v^2)}{dz} \tag{5a}$$

where τ_t^e and τ_t^e are the tangential and the normal forces, respectively, per unit area exerted on the surface of the jet due to E; τ_{zz} is the shear stress in the axial direction; g is the gravitational acceleration; and p is the pressure. Because the sum of the normal forces at the surface of the jet is equal to zero

$$p + \tau_n^e = \tau_{rr} + \frac{\gamma}{r} \tag{5b}$$

where τ_{rr} is the shear stress in the radial direction.

The Giesekus model adds quadratic nonlinearity and divides the deviatoric stress into a solvent contribution and a polymer contribution[26] as follows:

$$\tau = \tau_s + \tau_p \tag{5c}$$

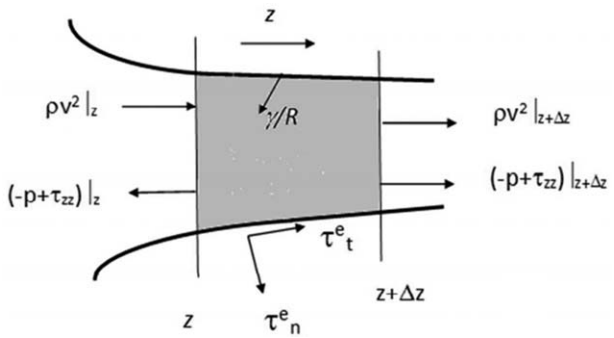

Figure 3. Forces applied to the chosen control volume.

where τ is the total shear stress, τ_p is the polymer shear stress, and τ_s is the solvent shear stress, which is deduced from the Newtonian constitutive law given by

$$\tau_s = 3\eta_s \frac{dv}{dz} \tag{5d}$$

where η_s is the solution viscosity. The τ_p equations are obtained from the viscoelastic laws[26] as follows:

$$\tau_{prr} + \lambda(v\tau'_{prr} + v'\tau_{prr}) + \alpha\frac{\lambda}{\eta_p}\tau^2_{prr} = -\eta_p v' \tag{5e}$$

$$\tau_{pzz} + \lambda(v\tau'_{pzz} - v'\tau_{pzz}) + \alpha\frac{\lambda}{\eta_p}\tau^2_{pzz} = 2\eta_p v' \tag{5f}$$

where α is the mobility factor; τ_{pzz} and τ_{prr} are the shear stresses of the polymer in the axial and radial directions, respectively; λ is the linear charge density in C/m; and η_p is the polymer viscosity. The prime symbol indicates the first derivative with respect to z.

With the substitution of eqs. (5b) and (2d-2f) into (5a), the momentum equation in the z direction[15] becomes

$$\frac{d(\rho r^2 v^2)}{dz} = 2r\varsigma E + \frac{T'_p}{\pi} + r'\gamma + r^2\left[\frac{\varsigma\varsigma'}{E} - (\bar{\varepsilon}-\varepsilon)EE'\right] + (3\eta_s v'\pi r^2) \tag{6}$$

where ε and $\bar{\varepsilon}$ are the permittivities of the jet and the air, respectively; T_p is the tensile force estimated by the multiplication of the shear stresses ($\tau_{pzz} - \tau_{prr}$) by the cross-sectional area of the jet (πr^2; and all parameters followed with a prime symbol indicate the first derivative with respect to z.

The equation for E was given by Reneker and Fong[15] as follows:

$$E(z) = E_\infty(z) + \ln\left(\frac{r}{L}\right)\left[1\bar{\varepsilon}\frac{d(\varsigma r)}{dz} - \frac{\beta}{2}\frac{d^2(Er^2)}{dz^2}\right] \tag{7}$$

where β is the permittivity ratio ($\bar{\varepsilon}/\varepsilon - 1$) and L is the jet length. The complete derivation of the stable jet model was given in Feng[12] and Reneker and Fong.[15]

Boundary conditions. At the onset of the electrospinning, the jet just outside of the nozzle has a radius r_0 and a velocity v_0. A ς boundary condition has been a longstanding problem in previous studies of electrospraying and electrospinning.[12] Hohman *et al.*[16] solved this problem by fitting the model predictions to the measurements and found that a steady solution was attained when only ς tended to zero at the onset of electrospinning. Thus, the zero charge density at the onset of the jet was adopted in this model. Because ς was null, I was only limited to the conductive part at the onset of the jet. Therefore, we deduced E from eq. (4) by neglecting the convective part. Finally, the shear inside the nozzle was assumed to be ineffective in stretching polymer molecules as compared with the elongation downstream, such that the stress at the onset of the jet was purely Newtonian.[13] At the final stage, the jet thinning was no longer considerable, and a zero gradient was then applied to r, the velocity, ς, and E. Therefore, the boundary conditions for the geometry, the velocity, and E are

$$r(z=0) = r_0 \quad \text{and} \quad \frac{dr(z=L)}{dz} = 0 \tag{8a}$$

$$v(z=0) = v_0 = \frac{Q}{\pi R_0^2} \quad \text{and} \quad \frac{dv(z=L)}{dz} = 0 \tag{8b}$$

$$E(z=0) = E_0 = \frac{I}{\pi r^2 k} \quad \text{and} \quad \frac{dE(z=L)}{dz} = 0 \tag{8c}$$

When the stable jet governing equations for the charge density are solved, the velocity, E as function of z, r_{sj}, and γ could be calculated. These two outputs were then used in the governing equations of the unstable jet. To our knowledge, this is the first time r_{sj}, γ, and L_{sj} [obtained iteratively from eq. (2)] have been used in the development of a model of the bending instability region of the second stage of the electrospinning process.

Bending Instability. Although electrospinning is a simple process to perform, the bending instability involves a complex interplay between the fluid dynamics, electrodynamics, and rheology. Because of this complexity, it is difficult to derive a mathematical model for the bending instability.[19] Therefore, we had to make a few assumptions that allowed the derivation of the expression that related the final fiber diameter to the electrospinning process and parameters. The jet was mainly treated as a slender viscous object. In addition, at the final stage of the whipping mode, r was decreasing, and competition was viewed between γ and the surface charge repulsion. Moreover, I from eq. (7) was reduced to the convective term at the final stage of electrospinning, and the conductive term was neglected. On the basis of the previous assumptions, Fridrikh *et al.*[20] presented a simple expression that relates the final fiber diameter to the influencing parameters on the basis of the equation of motion for the normal displacement ($\ddot{x}$) derived from Hohman *et al.*[22]

The model prediction arose from a force balance between γ and the electrostatic charge repulsion. The expression was then corrected by the concentration of the polymer in the solution. The model treats the jet as a slender viscous object. The equation of motion for $\ddot{x}$ (see Figure 2) of the jet centerline was presented by Hohman *et al.*[22] as follows:

$$\rho\pi r^2\ddot{x} = 2\pi\varsigma E_\infty\hat{\xi} + \left[\pi\gamma + \frac{r\bar{\varepsilon}}{2}\beta(E_\infty.\hat{t})^2 + 2\pi^2 r\varsigma^2\bar{\varepsilon}(3 - 2\ln\chi_{bi})\right]\frac{r}{R} \tag{9}$$

where $\hat{\xi}$ and $\hat{t}$ are the normal and the tangential directions, respectively, of the bending instability curvatures and R is the radius of curvature of the bending instabilities. The first term of eq. (9) accounts for the effect of E on the surface free charges of the jet. The second term is γ. The third term originates from the bending motion. The last term is the electrostatic repulsion. At the final stage of the whipping mode, r is decreasing, and

the competition is viewed between γ and the surface charge repulsion. Furthermore, at the late stage of whipping, eq. (3) is reduced as follows:

$$2\pi r\varsigma v = I \tag{10}$$

With eq. (2) and (10), the final fiber diameter at the final whipping stage leads to the expression of Frifrikh *et al.*[20] given by

$$r_f = 0.5\, C^{0.5}\left[\gamma\bar{\varepsilon}\frac{Q^2}{I^2}\frac{2}{\pi(2\ln\chi_{bi}-3)}\right]^{1/3} \tag{11}$$

where χ_{bi} is the ratio of the characteristic axial length scale. The previous expression is mostly limited to selective polymer–solvent system[19] and is applicable to the final stage of electrospinning when the competition is between the γ force and the electrostatic repulsion.[20] The expression of Frifrikh *et al.*[20] is not applicable to a relatively high polymer solution concentration higher than 12 wt % because of the relatively large viscous force dampers. Therefore, the viscous force cannot be neglected and the bending instabilities that occur are quite smooth.

χ_{bi} was defined by Hohman *et al.*[16,22] and is determined in practice by the shape of a jet as it thins away from the nozzle to r_{sj}. Thus, χ_{bi} is the wavelength [Ω (m)] estimated from the fastest growing mode of the spinning jet, and it leads to maximum thinning.[15] Therefore, the dimensionless parameter χ_{bi} appearing in eq. (11) is given by

$$\chi_{bi} = \frac{\Omega}{r_{sj}} \tag{12}$$

where r_{sj} is obtained from the solution of the governing equations of the stable jet region [eqs. (3-7)]. The maximum growth rate[18] (w_{max}) of R is calculated as follows:

$$w_{max} = \left(\frac{9\pi^4\varsigma_s}{r^2\mu}\right)^{1/3}[2\pi\rho\bar{\varepsilon}(2\ln\chi_{bi}-3)]^{1/6} \tag{13a}$$

where ς_s and μ are the surface charge density and the viscosity of the solution, respectively. On the other hand, Ω, shown in the χ_{bi} equation [eq. (12)], is estimated from the wave number (K) of the instabilities occurring in the stable jet[15] as follows:

$$\Omega = \frac{2\pi}{K} \tag{13b}$$

The equation of K was derived by Reneker *et al.*[15] through the balancing of the forces resulting from ς and η_s. This equation corresponds to w_{max} of the bending instabilities and presents a strong link between the stable and the unstable regions. The reason is that the K equation is a function of the two stable jet outputs: r_{sj} and ς_{sj} at L_{sj}. The K equation[15] becomes

$$K = \left(\frac{\pi^2\varsigma_{sj}}{r_{sj}^2\mu}\right)^{1/3}[2\pi\rho\bar{\varepsilon}(2\ln\chi_{bi}-3)]^{1/6} \tag{13c}$$

As K depends on the χ_{bi} parameter, iterations are needed to find the convergent χ_{bi} required to determine the final radius (r_f), with eq. (11). The coupling between the stable jet and the bending instability stage occurs with r_{sj} and ς_{sj} to determine χ_{bi}. The novelty of the method arises from this coupling, which combines several validated models to generate a simplified model. This simplified model relates the electrospinning parameters to the final fiber diameter. In other words, the model of Fridrikh *et al.*[20] is modified by the calculation of χ_{bi} on the basis of Hohman *et al.*'s[16,22] definition and with the equations developed by Reneker *et al.*[15] These equations are related to the first stage of electrospinning (the stable jet) based mainly on the work of Feng.[12] Fridrikh *et al.*[20] stated a range for χ_{bi} between 10 and 1000 but used a value of 100 at a final fiber diameter of 100 μm. It was interesting to accurately calculate the parameter χ_{bi} as a function of the stable jet region parameters to improve the accuracy of the predictions of the final fiber diameter at the desired distance of the bending instability region.

Numerical Solution. Figure 4 shows the flow chart of the model numerical approach. The coupled eqs. (3-7) with the associated boundary conditions given in eqs. (8-10) were discretized with a finite volume methodology, where the electrospinning jet was divided into a number of grids (N_z) with a circular cross section and a grid size of Δz. Central differencing was used for second-order terms. The input set divided on the solution properties and processing parameters were used in the model. The L_{sj} value was assumed, and Δz was calculated on the basis of a constant N_z of 366. Afterward, initial guesses for r, ς, E, and v for all nodes were assumed and iterated until convergence with a maximum relative error of 10^{-5}. Once all these unknowns were predicted for all nodes, the r_{sj}, ς_{sj}, stable jet electric field (E_{sj}), and stable jet velocity (v_{sj}) were used to calculate L_{sj}, as given in eq. (2). Thus, the calculation was repeated, and an updated L_{sj} was predicted. The calculation of L_{sj} was also repeated until convergence with a maximum relative error of 10^{-5} occurred. The numerical solution was repeated for different grid sizes to ensure that a grid-independent solution was obtained. In the presented simulations, the number of grid points was 366 in the jet direction with Δz depending on L_{sj}.

The coupling between the stable jet and the bending instability region occurred with r_{sj} and ς_{sj} in the bending instability equations [eqs. (11-13c)]. First, Ω was assumed, and then, the dimensionless parameter χ_{bi} was calculated on the basis of eq. (12) with r_{sj}. After that, the wave number was calculated on the basis of the dimensionless parameter χ_{bi} and ς_{sj}. Then, the corresponding Ω was recalculated and compared to the assumed one. The calculation is repeated until a Ω convergence was achieved with a maximum relative error of 10^{-5}. Finally, r_f of eq. (11) was calculated.

Experimental Methodology

Materials. PAN, with an average molecular weight of 150,000 g/mol, and *N*,*N*-dimethylformamide (DMF; ≥ 99.8%, American Chemical Society spectrophotometric grade) were purchased from Sigma-Aldrich and were used as received without further purification.

Preparation of the PAN Nanofibers. PAN polymeric solutions at different weight concentrations were prepared by the dissolution of PAN powder in DMF under constant magnetic stirring at 900 rpm for 24 h at room temperature.[28] To remove the entrapped air bubbles, the polymeric solutions were sonicated in a Cole-Parmer 8851 sonication bath at 47 kHz for about 20 min before the electrospinning process. A laboratory-scale

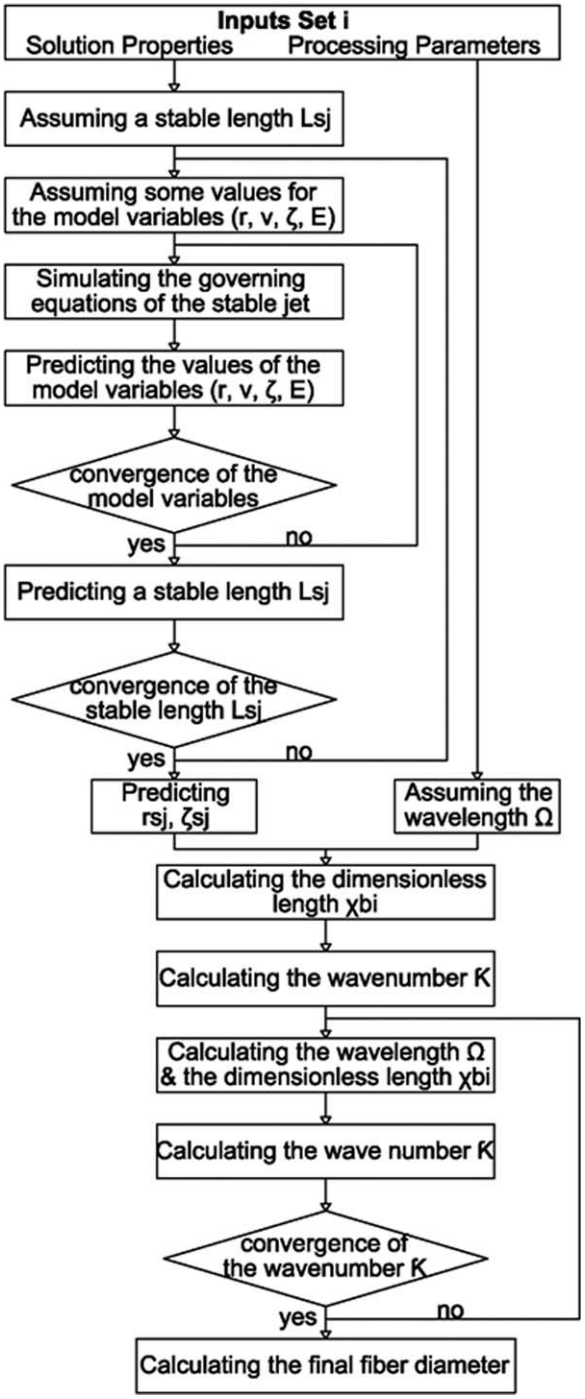

Figure 4. Flow chart of the complete model.

electrospinning machine (Fluidnatek LE-10, Bioinicia, Spain) was used for the preparation of the PAN nanofibers (Figure 5). The inner and outer diameters of spinneret nozzle were 0.6 and 0.9 mm, respectively. The collector was a rotating drum (100 mm diameter × 200 mm length) made of anodized aluminum covered by a piece of aluminum foil, with a variable rotational speed from 200 to 2000 rpm. By specifying Q, the applied voltages (0–30 kV), the tip-to-collector distance, and the velocity of the collector drum, we generated a horizontal E between the nozzle and the collector. This E allowed the jet to leave the nozzle and to be stretched horizontally. The electrospun nanofibers were collected at a controlled room temperature of 20 °C and at 30% relative humidity.[29]

***I* Measurement.** To find the current correlation, I needs to be measured for different electrospinning conditions. For this measurement, one can measure the voltage drop across a resistor that is in series with the grounded collector with Ohm's law.[23] As I during electrospinning is on the order of nanoamperes to microamperes, a resistance of high impedance (20 MΩ) and a regular voltmeter (Fluke 117 multimeter) were used.

Fiber Diameter Measurement. Morphological observation of electrospun samples was performed with a scanning electron microscope (Mira 3 LMU Tescan) operating at an acceleration voltage of 15 kV with a working distance of 3 mm with an InBeam detector at a magnification range from 3000 to 50,000×. For each electrospun web, five circular specimens were cut from different places, and 20 fiber measurements were conducted for each specimen. Accordingly, 100 measurements were averaged with their proper standard deviation with the Mira built-in measurement software.

PAN solutions with various weight concentrations were electrospun under the ambient conditions of 20 °C and a relative humidity of about 30%. Different sets of experiments were performed where one parameter was varied in each set, as shown in Table I. In the first set, Q was varied from 900 to 1320 μL/h, whereas E and the polymer concentration were kept constant at 97,222 V/m and 10 wt %. The aim of this set is to figure out the effect of solution Q on the final fiber diameter. In the second set, E was varied from 88,889 to 113,889 V/m, whereas the Q and the polymer concentration were kept constants at respectively 900 μL/h and 10 wt %. In these experiments, we examined the influence of increasing E on the final fiber diameter. Finally, in the third set, the polymer concentration was varied from 8 to 11 wt %, whereas E and Q were

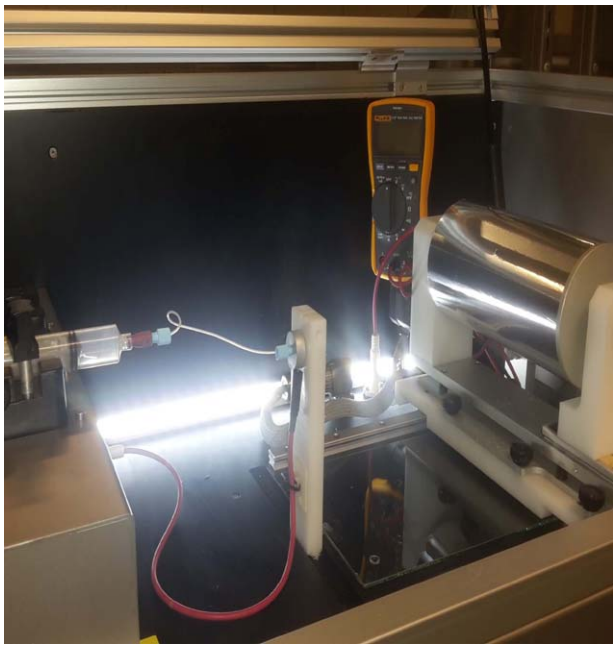

Figure 5. Electrospinning device used. [Color figure can be viewed in the online issue, which is available at wileyonlinelibrary.com.]

Table I. Parameters for the Set of Experiments Performed

			Solution property	
	Q (μL/h)	E (V/m)	Concentration (%)	Conductivity (mS)
Varying Q	900	97,222	10	8232
	960	97,222	10	8232
	1020	97,222	10	8232
	1080	97,222	10	8232
	1140	97,222	10	8232
	1200	97,222	10	8232
	1260	97,222	10	8232
	1320	97,222	10	8232
Varying E	900	88,889	10	8232
	900	91,667	10	8232
	900	94,444	10	8232
	900	97,222	10	8232
	900	100,000	10	8232
	900	102,778	10	8232
	900	105,556	10	8232
	900	108,333	10	8232
	900	111,111	10	8232
	900	113,889	10	8232
Varying polymer concentration	900	97,222	8	726524
	900	97,222	9	778994
	900	97,222	10	823204
	900	97,222	11	859154

kept constant at 97,222 V/m and 900 μL/h, respectively. In these experiments, we aimed to establish the profile of the final fiber diameter against the polymer concentration. All of the electrospinning parameters were chosen in a range that ensured generation of a continuous jet without droplets.[29]

For each experiment, I was measured, and five different samples from different parts of the final web were studied by scanning electron microscopy (SEM) to measure the final fiber diameter and its distribution (see Figure 6). The measured I was used to calculate a from eq. (1) (see the Appendix). The I equation [eq. (1)] was used in the model.

RESULTS AND DISCUSSION

The model was simulated for the three experiment sets summarized in Table I, and the final fiber diameter was calculated. To ensure the validity of the model predictions, the calculated and the experimental fiber diameters were subject to the same conditions. The relative error between them is reported for each simulation.

Figure 7(a–c) shows the theoretical and experimental fiber diameters as a function of Q, E, and the polymer concentration. The error bars shown in Figure 7 are related to the standard deviation given by the SEM machine. The average standard deviation was about ±32 nm. There was good agreement between the predicted and experimental values, with an average relative error of 6.65% and a maximum relative error of 10%.

Effect of Q on the Fiber Diameter

Our model predictions agreed with the experimental fiber diameters at different Qs, with a relative error of 6.5%. The final fiber diameter increased with increasing Q; this is the case for most polymeric solutions [see Figure 7(a)].[30] This was similar to the fiber diameter trend reported in the literature,[31] where at small Qs, a small amount of solution was ejected from the nozzle. With increasing Q at the same E, a larger amount of solution volume was ejected. However, E_∞ was not capable of stretching the ejected solution with a larger volume. This limited stretching led to an increase in the fiber diameter at a larger Q. Moreover, it was shown that Q had a significant effect on the final diameter: an increase of 30% in Q led to an increase of 15% in the fiber diameter.

Effect of E on the Fiber Diameter

Figure 7(b) shows the variation of the fiber diameter with E. The figure shows the good agreement between the model predictions and the experimental results, which showed an average relative error of 6.72%. Moreover, it clearly illustrates that the increase of E yielded a decrease in the fiber diameter. Indeed, the increase in the applied E yielded an increase in the drawing force (Coulombic force), which was responsible for the stretching and thinning of the fiber. Therefore, an increase in E contributed to the decrease in the final fiber diameter. For instance, an increase of 30% in E yielded a decrease of 14% in the final fiber diameter.

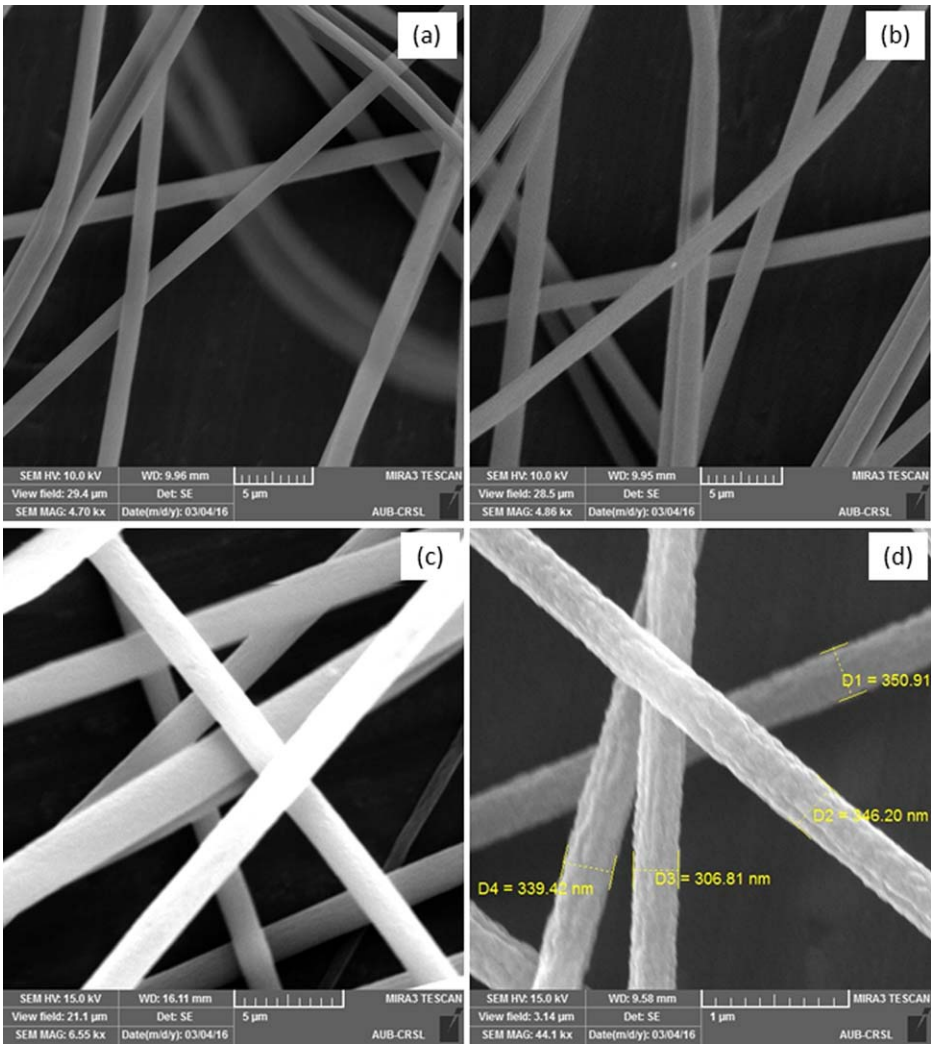

Figure 6. Sample SEM images: (a) $Q = 900\ \mu L/h$, $E = 97{,}222\ V/m$, and $C = 10\%$; (b) $Q = 900\ \mu L/h$, $E = 88{,}889\ V/m$, and $C = 10\%$; and (c) $Q = 900\ \mu L/h$, $E = 97{,}222\ V/m$, and $C = 11\%$ and (d) fiber diameter measurements for Q = 900 micro L/h, E = 97,222 V/m, and C = 11%. C: Polymer Concentration; D1: fiber diameter measurement 1; D2: fiber diameter measurement 2; D3: fiber diameter measurement 3; D4: fiber diameter measurement 4. [Color figure can be viewed in the online issue, which is available at wileyonlinelibrary.com.]

Effect of the Polymer Concentration on the Fiber Diameter

Figure 7(c) shows the variation of the fiber diameter with the polymer concentration. The model predictions agreed with the experiment measurements of the final fiber diameter, with an average error of 6.72%. The effect of the concentration on the fiber diameter is generally related to the viscous effect. As the polymer concentration increases, η increases. However, the viscous force stands against the stretching of the fiber. Consequently, the fiber diameter increased with increasing η.[28] In other terms, an increase in the concentration led to an increase in the final fiber diameter. However, the effect of concentration was negligible compared to the effects of Q and E. As shown in Figure 7(c), an increase of 30% in the concentration contributed to only a 1% increase in the fiber diameter.

Model Validation with a Published Experimental Study

Ozkok *et al.*[32] investigated the effect of the solution concentration on the morphology of the PAN nanofibers by measuring the fiber diameter at different concentrations. In this section, we are interested in comparing our model results with those of Ozkok *et al.*'s[32] published experiment. Unlike other studies, Ozkok *et al.*[32] provided all of the electrospinning parameters needed as input to validate our model. These parameters were as follows: $r_0 = 0.7$ mm, $\Delta V = 35$ kV, $Q = 0.5$ mL/h, and $L = 10$ cm. The fiber diameter varied from 216 nm at a polymer concentration of 6 wt % to 270 nm at a polymer concentration of 12 wt %. With the same input, our model predicted the same trend with a maximum relative error of 15%. The predicted fiber diameter varied from 189 to 230 nm at polymer concentrations of 6 to 12 wt %, respectively. Because the standard deviation of SEM measurement was about ± 32 nm, the predicted fiber diameter with our model was within the range of the published experiment.

Model Comparison against the Predictions of Published Models

Even though the stages of electrospinning have been investigated in the literature with different mathematical models, the developers of these models were mainly interested in studying the jet profile, the

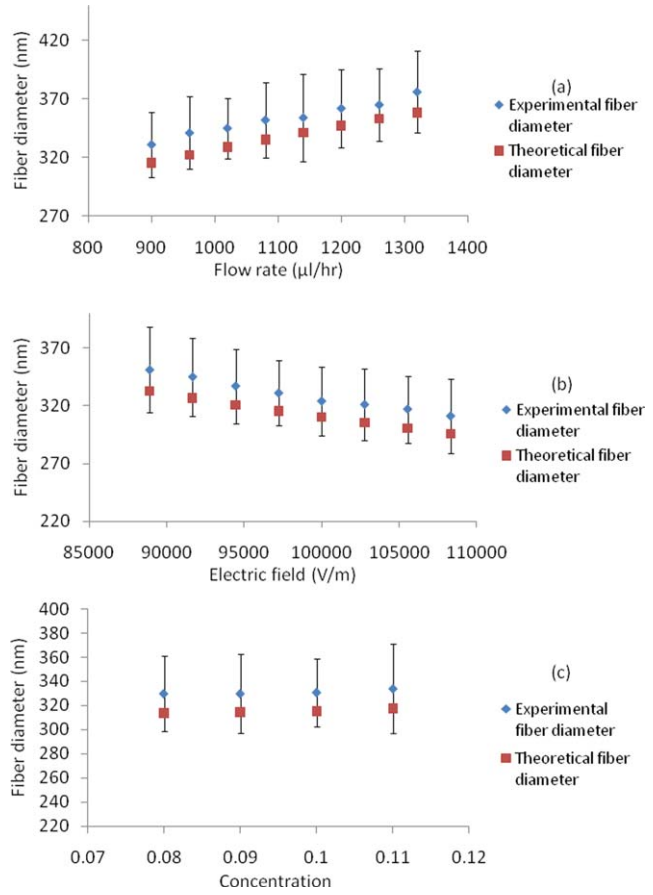

Figure 7. Comparison of the theoretical and experimental fiber diameters for (a) different *Q*s, (b) different *E*s, and (c) different concentrations. [Color figure can be viewed in the online issue, which is available at wileyonlinelibrary.com.]

stability of the jet, and the physics behind the bending instabilities.[8] Few models show the final fiber diameter explicitly.[20] For instance, some authors have presented scaling studies of the final fiber diameter in electrospinning as function of the processing parameters and did not come up with the fiber diameter values.[19] Other models, such as that of Zeng *et al.*[33] and Stepanyan *et al.*,[34] which were based on published physical models, predict the final fiber diameter at different processing parameters. However, they did not report their model accuracy. Fridrikh *et al.*[20] reported an average relative error of 20% for a PAN solution compared to a relative error of 6.65% in our model. The main reason was that Fridrich *et al.*[20] used an arbitrary range for χ without developing a systematic method for its calculation. However, in this study, χ was related to the first electrospinning stable jet stage; this coupled the stable and the unstable jet regions and led to more accurate fiber diameter prediction.

The main feature of our model is its fast convergence because it combines numerical and analytical methods for the prediction of the final fiber diameter. The rate of convergence varied between simulations; thus, an average time convergence is reported. For the stable jet region, L_{sj} needed about 20 iterations to converge. In each iteration, r_{sj} and ς_{sj} were calculated after approximately 200 iterations. For the unstable jet model, the number of iterations needed for χ_{bi} to converge was about 40 iterations. Thus, the total time needed in each simulation to predict the final fiber diameter was approximately a few minutes with a four-core computer and 3.2 GHz of random access memory. The developed model is simple and predicts the fiber diameter at comparable accuracy to that of a more complex and computationally expensive model that uses a Lagrangian approach, in which the charged particles are followed in the unstable jet region.[18,19]

Model Limitations

The main limitation of this model was attributed to the assumption used to come up with the final fiber diameter correlation [eq. (11)] in the bending instability region. This assumption limits the model to relatively small polymer–solvent concentration ($\leq$12 wt %). Another limitation is related to the collection speed. In this study, we chose an average collecting speed of 600 rpm.[29] The choice of this collection speed was basically related to the fact that a high collecting speed can affect the final fiber diameter; this was the result of the force exerted on the depositing fibers by the take-up roll.[35]

CONCLUSIONS

In this study, a simplified and accurate model of electrospinning was developed to predict the final fiber diameter. The model couples the two electrospinning stages to relate the electrospinning parameters to the final fiber diameter. We achieved the validation of the model by performing a set of experiments at different electrospinning processing conditions. The developed model succeeded in evaluating the fiber diameter at different processing parameters and presented a relatively high accuracy (average relative error = 6.65%) compared to other models (average relative error = 20%). The fiber diameter increased with increasing *Q* and concentration and decreased with increasing *E*. This study will be followed by further studies that use the final fiber diameter in the estimation of the morphological properties, such as thickness, air permeability, and porosity, of the nanofiber web collected. These morphological properties are important in textile applications, particularly in protective clothing, where the unique characteristics of the nanofiber web, such as the large surface-area-to-volume ratio and low basis weight, can be used for full-scale air filtration applications in toxic environments.

ACKNOWLEDGMENTS

The authors acknowledge the financial support of the Lebanese National Council for Scientific Research (project award 103061-22909).

APPENDIX: ELECTRIC CURRENT CORRELATION

The electric current was measured in electrospinning scales as $E_\infty Q^{0.5} k^{0.4}$ for wide polymer solutions in an organic solvent. Thus, we predicted the electric current from eq. (1) by finding the average *a* for the PAN/DMF solution. Therefore, each *E*, *Q*, and conductivity were varied. For an *E* of 97,222 V/m and an electrical conductivity of 0.0082 S (corresponding to a concentration of 10%), the experiment was repeated eight times for

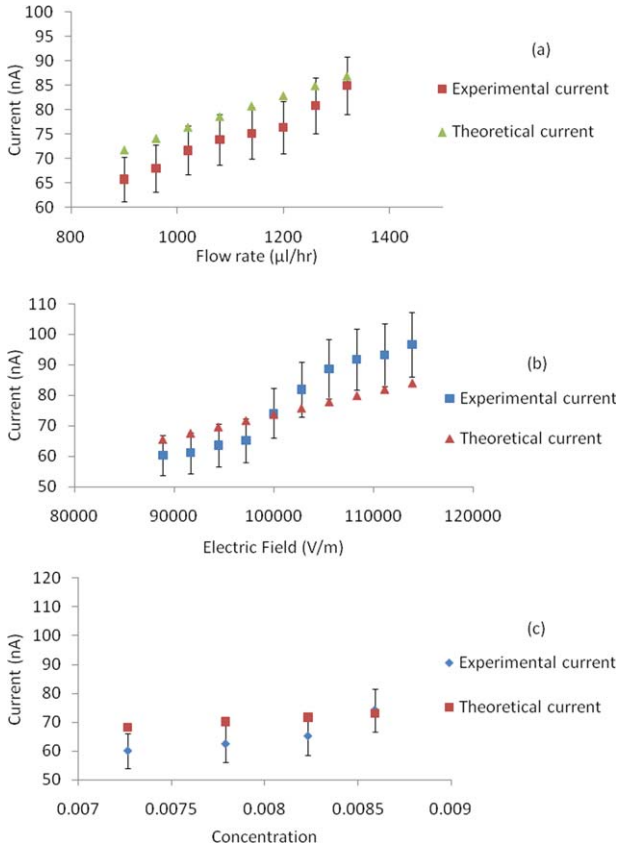

Figure A1. Comparison of the theoretical and experimental currents for (a) different *Q*s, (b) different *E*s, and (c) different electrical conductivities. [Color figure can be viewed in the online issue, which is available at wileyonlinelibrary.com.]

different *Q*s, ranging from 900 to 1320 μL/h. Furthermore, for a *Q* of 900 μL/h and an electrical conductivity of 0.0082 S (corresponding to a concentration of 10%), the experiment was repeated 10 times for different *E*s ranging from 88,889 to 113,889 V/m. Finally, for a *Q* of 900 μL/h and an *E* of 97,222 V/m, the experiment was repeated eight times for different electrical conductivities ranging from 0.0072 to 0.0085 S (corresponding to a concentration ranging from 8 to 11%). For each experiment, *a* was found, and the average of all constants was used in the correlation. The experiments show an average constant of 3.182×10^{-7} with a maximum relative error of 14%. Equation (1) becomes

$$I = 3.182 \times 10^{-7} \times E_{\infty} Q^{0.5} k^{0.4} \quad \text{(A.1)}$$

Figure A1(a–c) compares the experimental and theoretical currents occurring with different *Q*s, different *E*s, and different electrical conductivities. The error bars in Figure 1 are related to the standard deviation of the experiments caused mainly by the multimeter fluctuation. Good agreement was observed between the experimental and theoretical currents, with an average relative error of 9% and a maximum relative error of 14%. On the other hand, the theoretical electric current values were in the range of published articles. For instance, the electrical current in the work of Barua and Saha[29] was approximately in the same range of our electrical current, even though electrospinning could be achieved at different r_0 values of the nozzle (depending on the geometrical parameters of the electrospinning machine).

REFERENCES

1. Frenot, A.; Chronakis, I. S. *Curr. Opin. Colloid Interface Sci.* **2003**, *8*, 64.
2. Schreuder, G. H.; Gibson, P.; Senecal, K.; Sennett, M.; Walker, J.; Yeomans, W.; Ziegler, D.; Tsai, P. P. *J. Adv. Mater.* **2002**, *34*, 44.
3. Wang, Y.; Serrano, S.; Santiago-Aviles, J. *J. Mater. Sci. Lett.* **2002**, *21*, 1055.
4. Warner, S. B.; Buer, A.; Grimler, M.; Ugbolue, S. C.; Rutledge, G. C.; Shin, M. Y. 1999 Annual Report (M98-D01); National Textile Center: **1999**. Blue Bell, PA, USA.
5. Ji, Y.; Li, B.; Ge, S.; Sokolov, J. C.; Rafailovich, M. H. *Langmuir* **2006**, *22*, 1321.
6. Mohan, A. Formation and Characterization of Electrospun Nonwoven Webs. http://www.lib.ncsu.edu/resolver/1840.16/1925. (Accessed December 1, 2015).
7. Shi, X.; Zhou, W.; Ma, D.; Ma, Q.; Bridges, D.; Ma, Y.; Hu, A. J. Nanomater. **2015**, *2015*, 1–20.
8. Rafiei, S.; Maghsoodloo, S.; Noroozi, B.; Mottaghitalab, V.; Haghi, A. K. *Cellul. Chem. Technol.* **2013**, *47*, 323.
9. Sarkar, K.; Hoos, P.; Urias, A. *J. Nanotechnol. Eng. Med.* **2012**, *3*, 041001.
10. Taylor, G. *Proc. R. Soc. London A* **1969**, *313*, 453.
11. Gupta, P. Processing-Structure-Property Studies of: I) Submicron Polymeric Fibers Produced By Electrospinning and II) Films Of Linear Low Density Polyethylenes As Influenced By The Short Chain Branch Length In Copolymers Of Ethylene/1-Butene, Ethylene/1-Hexene & Ethylene/1-Octene Synthesized By A Single Site Metallocene Catalyst. PhD Thesis, Virginia Polytechnic Institute and State University, USA, **2004**.
12. Feng, J. *Phys. Fluids* **2002**, *14*, 3912.
13. Roozemond, P. C., A Model for Electrospinning Viscoelastic Fluids. Bachelor Final Project, Eindhoven University of Technology, Department of Mechanical Engineering. Report No. MT07.12, , Eindhoven, Netherlands, **2007**.
14. Helgeson, M. E.; Grammatikosa, K. N.; Deitzelb, J. M.; Wagnera, N. J. *Polymer* **2012**, *49*, 2924.
15. Reneker, D. H.; Fong, H. Polymeric Nanofibers. **2005**, ACS Symposium Series 918, American Chemical Society, Washington, DC, USA.
16. Hohman, M. M.; Shin, M.; Rutledge, G.; Brenner, M. P. *Phys. Fluids* Part I, **2001**, *13*, 2201.
17. Yarin, A. L. *Polym. Adv. Technol.* **2011**, *22*, 310.
18. Reneker, D. H.; Yarin, A. L.; Fong, H. *J. Appl. Phys.* **2000**, *87*, 4531.
19. Gadkari, S. *SpringerPlus* **2014**, *3*, 705.
20. Fridrikh, S. V.; Jian, H. Y.; Brenner, M. P.; Rutledge, G. C. *Phys. Rev. Lett.* **2003**, *90*, 144502.

21. Subbotin, A.; Stepanyan, R.; Chiche, A.; Slot, J. J. M.; Ten, B. G. *Phys. Fluids* **2013**, 25, 103101.
22. Hohman, M. M.; Gregory, R.; Michael, P. *Phys. Fluids*, Part II, **2001**, *13*, 2201.
23. Carroll, C. P.; Joo, Y. L. Phys. Fluids **2006**, *18* (5), 053102.
24. He, J. H.; Wan, Y. Q.; Yu, J. Y. *Polymer* **2005**, *46*, 2799.
25. Bhattacharjee, P. K.; Schneider, T. M.; Brenner, M. P.; McKinley, G. H.; Rutledge, G. C. *J. Appl. Phys.* **2010**, 107, 044306.
26. Hinch, E. Lecture 2: Constitutive Relations. https://www.whoi.edu/fileserver.do?id=28326&pt=10&p=17274. Accessed on August 30, 2015.
27. He, J. H.; Wu, Y.; Zuo, W. W. *Polymer* **2005**, *46*, 12637.
28. Gomes, D. S.; da Silva, A. N.; Morimoto, N. I.; Mendes, L. T.; Furlan, R.; Ramos, I. *Polímeros* **2007**, *17*, 206.
29. Barua, B.; Saha, M. *J. Appl. Polym. Sci.* **2015**, *132*, DOI: 10.1002/app.41918.
30. Subbiah, T.; Bhat, G. S.; Tock, R. W.; Parameswaran, S.; Ramkumar, S. S. *J. Appl. Polym. Sci.* **2005**, *96*, 557.
31. Zargham, S.; Bazghir, S.; Tavakoli, A.; Rashidi, A. S.; Damerchely, R. *J. Eng. Fiber Fabr.* **2012**, *7*, 42.
32. Ozkok, U.; Icoglu, H. I.; Kirecci, A. *J. Mater. Sci. Eng.* **2011**, *5*, 227.
33. Zeng, Y.; Pei, Z.; Wang, X. Proceedings of the 8th WSEAS International Conference on Applied Computer and Applied Computational Science; Hangzhou, China, May 20–22, **2009**, China Jiliang University & Zhejiang University of Technology.
34. Stepanyan, R.; Subbotin, A.; Cuperus, L.; Boonen, P.; Dorschu, M.; Oosterlinck, F.; Bulters, M. *Appl. Phys. Lett.* **2014**, *105*, 1.
35. Sutasinpromprae, J.; Jitjaicham, S.; Nithitanakul, M.; Meechaisue, C.; Supaphol, P. *Polym. Int.* **2006**, *55*, 825.